Mediterranean Marine Science

Vol 12, No 1 (2011)

A 2-year intercomparison of the WAM-Cycle4 and the WAVEWATCH-III wave models implemented within the Mediterranean Sea

G. KORRES, A. PAPADOPOULOS, P. KATSAFADOS, D. BALLAS, L. PERIVOLIOTIS, K. NITTIS

doi: 10.12681/mms.57

Mediterranean Marine Science
Indexed in WoS (Web of Science, ISI Thomson)
The journal is available on line at http://www.medit-mar-sc.net

Research Article

A 2-year intercomparison of the WAM-Cycle4 and the WAVEWATCH-III wave models implemented within the Mediterranean Sea

G. KORRES[1], A. PAPADOPOULOS[1], P. KATSAFADOS[2], D. BALLAS[1], L. PERIVOLIOTIS[1] and K. NITTIS[1]

[1] Hellenic Centre for Marine Research, P.O. Box 712, 19013 Anavissos, Hellas
[2] Department of Geography, Harokopio University of Athens, Hellas

Corresponding author: gkorres@ath.hcmr.gr

Received: 22 April 2010; Accepted: 8 February 2011; Published on line: 18 April 2011

Abstract

In this work we present the implementation of a wave forecast/hindcast system for the Mediterranean Sea at a 1/10° horizontal resolution and we show a first assessment of its performance by inter-comparing model results to observational data time series at selected points for the period 2000-2001. The system which is part of the POSEIDON-II operational system includes the WAM – Cycle4 and the WAVEWATCH-III wave forecast models (implemented within the same region) one way coupled with the non-hydrostatic version of the ETA atmospheric model, which provides the necessary wind velocity fields to the wave models at 3-hour intervals. The same system, but based on the WAM-Cycle4 wave model, has been used in the past for the production of the Aegean Sea wind and wave Atlas. Overall, the inter-comparison shows that both wave models are rather skilful in predicting the integral wave parameters with significant wave height skill scores in the range 0.85-0.90 and mean period scores in the range 0.77-0.83. It is also evident that the WAM model has a tendency to overestimate mean wave periods, while the opposite is true for the WAVEWATCH-III model. Differences between the two models simulated spectra exist along the main passage of cyclonic systems over the Mediterranean Sea, while in the wind seas dominated areas of the basin (the Aegean Sea for example) the two models show almost the same behavior.

Keywords: Mediterranean Sea; WAM; WAVEWATCH; Wave modeling; POSEIDON system.

Introduction

The proper knowledge of wave climate parameters, their associated trends and variability are of great importance for numerous human related marine activities such as safe navigation, search and rescue, shoreline erosion, sediment transport, coastal/open sea operations etc. Lately, the very interesting issue of wave driven ocean circulation and the transformation of the Navier-Stokes primitive equations, in order to include the effect of the Stokes drift has been put forward by several works, such as

MELLOR (2003); PERRIE *et al.* (2003); ARDHUIN *et al.* (2008). The surface waves affect the air-sea momentum exchange and thus the estimation of the drag coefficient and the wind stress at the sea surface that drives a large part of the ocean circulation (Ekman transport). There have been several indications, either experimental or theoretical, that the stage of development of the wind sea drastically modifies the wind stress at the sea surface, with important implications for proper storm surge forecasting. In a typical evolution of a storm, the peak period of the wave spectrum is initially rather short with high values of the surface drag coefficient. As the peak shifts to the lower part of the spectrum the value of the drag coefficient decreases rapidly. Therefore the drag depends not only on the local wind speed as most hydrodynamic and storm surge models assume, but also on the distortion of the sea surface. Beyond these aspects, the knowledge of the wave climate is a key point in climate studies that focus on air-sea interaction. Ocean waves are a natural integrator of the wind fields and therefore changes in the wind climate can be traced back from changes in the wave climate. On the other hand, the study of trends and variability of surface waves is interesting on its own as there are several facts nowadays indicating that during recent decades the global wave climate has undergone important changes.

A wave forecasting/hindcasting system for coastal or open sea areas is usually based on a wave generation model, on or offline, coupled with an atmospheric forecasting model that provides the necessary input terms (wind speed) to the wave model. Several systems are equipped with data assimilation machinery that merges wave forecasts with satellite or buoy wave measurements into analysis or re-analysis products. The present paper describes and assesses the performance of WAM–Cycle4 (WAM4) and WAVEWATCH-III (WW3) wave models adapted to the Mediterranean Sea, as they are both part of the POSEIDON-II operational system (NITTIS *et al.,* 2005).

The Mediterranean Sea is a semi enclosed basin with complicated geometry extending from 7°W to 36°N and from 30.25°N to 45.75°N. In several studies, it has been considered as a suitable test basin for a series of studies dealing with the general oceanic circulation problem. The Mediterranean basin is surrounded by a rather complicated system of mountain chains ranging between 1,500 m and 4,800 m height. Such orography distorts large synoptic systems, producing local winds such as the Etesians, the Bora and the Mistral, which can prevail almost throughout the year. Surface wave dynamics are expected to be conditioned by such wind regimes. The Mediterranean region is characterized by intense synoptic scale activity with features which, though their amplitude is smaller than that of the Atlantic and Pacific regions, are evident in the global storm track structure. In fact, the Northern Hemisphere storm track presents a separate branch crossing the Mediterranean region, with areas of cyclogenesis in the Western Mediterranean and of prevalent cyclolysis in the Central and Eastern Mediterranean.

From the wave modeling perspective, the Mediterranean Sea has a very complicated morphological structure. The complicated coastline, the protruding peninsulas, and the various large islands split the Mediterranean basin into a number of subbasins of smaller dimensions. Moreover, in areas like the Aegean Sea, the numerous islands, the complicated bottom topography, the presence of channels and related wave channelling phenomena (occurring

especially in the Dardanelles, the Crete - Antikythira and the Crete - Karpathos straits) present further difficulties in atmospheric and wave modeling efforts. For example a direct effect of the islands is the blocking of propagation and generation of waves on the lee side, reducing in this way the significant wave height and changing the peak period as compared with the general wave field. On the sheltered zones behind the islands, the wave field is expected to be dependent on the local wind. It is then well known that forecasting errors can be significant where the wind blows off the land, with a trend to decreasing with fetch (length of sea run by wind), approaching the correct values after several hundreds of kilometers. In an enclosed sea practically all the marine areas are in this situation, and the model values turn out to be underestimated. The wave heights, strongly connected to the driving winds, can be underestimated as well. The crucial role of the orography in shaping the wind fields and the need for higher-resolution models is then established. Owing to the strong dependence of wave height on the wind speed, coarse resolution atmospheric forecasts can be useless for an efficient evaluation of the wave conditions. It is expected that limited area, high resolution meteorological models (LAM) can alleviate much of the problem described above.

The wave forecasting/hindcasting system that is presented in this work mixes different scales of wave phenomenology and variability: the basin and the coastal scale. This is an interesting characteristic of the system which differs from other operational forecasting systems run by national met-offices and developed to predict/hindcast waves in open waters. The system has been developed as part of the POSEIDON II operational system running at the Hellenic Centre for Marine Research (HCMR) and premises producing daily 5-day weather, sea state, sea circulation and ecosystem functioning forecasts for the Mediterranean and the Aegean Seas. Almost the same system has been used in the past for the production of a 10-year Wind and Wave Atlas for the Hellenic Seas (SOUKISSIAN *et al.,* 2007) and will be used in the future for longer term hindcast simulations in order to study Mediterranean wave climate variability.

The WAM model which is one of the main constituents of the HCMR wave forecasting system, is a third generation wave model, which computes spectra of random short-crested wind-generated waves (HASSELMANN, 1988). The WAM model was the first model that solved the complete action density equation, including nonlinear wave-wave interactions. First and second generation wave models performed reasonably well in many cases but generally failed to give a proper description of the sea state in rapidly varying conditions. However the solution of the energy balance equation requires considerable computing power, which has become available in recent years. Third generation wave models have solved two basic problems. First, they have incorporated a parameterization of the exact nonlinear transfer source function (computations of the exact five-dimensional integral representing the continuum of all resonant interactions for the entire spectrum are still too time consuming for present-day computers). Second, they achieved a closure for the energy balance equation by better parameterizations of the dissipation source function. The dissipation function used in WAM corresponds to the form proposed by KOMEN *et al.* (1984) and is tuned to reproduce the observed fetch-limited wave growth and the fully developed Pierson-Moskowitz spectrum (PIERSON & MOSKOWITZ, 1964). In all, the WAM

model code propagates the wave spectrum in time and space, taking into account wave generation by the wind, wave shoaling and refraction due to depth and/or currents, quadruplet wave-wave interactions and finally bottom friction and white-capping. Nowadays, the WAM model is used operationally in many global and regional applications, producing forecasts of the sea state which can be used for many applications such as ship routing and offshore activities. Finally, much progress has been made in the assimilation of satellite observations into wave models. However, data assimilation is out of the scope of the present paper.

The paper is organized in the following way. In section 2 we give a rather extended presentation of the WAM model, while the WW3 model is briefly described in section 3. The setup of the mediterranean wave hindcast/forecast system is discussed in section 4. Section 5 deals with the analyses of wave model simulations over the period 2000-2001 and their assessment with respect to observed data. Finally a summary of the main findings of this work is offered in section 6.

The WAM model formulation

The evolution of the 2-D ocean wave spectrum $N(f,\theta,\varphi,\lambda,t)$ with respect to frequency f and direction θ (measured clockwise relative to true north) as a function of latitude φ and longitude λ on the spherical earth is dictated by the transport equation:

$$\frac{\partial N}{\partial t} + \frac{1}{\cos\varphi}\frac{\partial}{\partial\varphi}(\dot{\varphi}\cos\varphi) + \frac{\partial}{\partial\lambda}(\dot{\lambda}N) + \frac{\partial}{\partial\theta}(\dot{\theta}N) = S \qquad (1)$$

where is S the net source function describing the change of energy of a propagating wave group and

$$\dot{\varphi}\frac{d\varphi}{dt} = uR^{-1}\cos\theta \qquad (2)$$

$$\dot{\lambda}\frac{d\lambda}{dt} = v(R\cos\varphi)^{-1}\sin\theta \qquad (3)$$

$$\dot{\theta}\frac{d\theta}{dt} = v\tan\varphi\, R^{-1}\sin\theta \qquad (4)$$

represent the rates of change of the position and propagation direction of a wave packet traveling along a great circle path. The group velocity v is equal to $g/4\pi f$ and R is the earth radius. The above equations apply for wave propagation in water of infinite depth. For the finite depth case, modifications need to be introduced in the expression for the group velocity in the refraction equation (4) and in the form of the source function.

Source functions

The source function for the deep water case may be represented as a superposition of the wind input, nonlinear transfer and white capping dissipation source functions,

$$S = S_{in} + S_{nl} + S_{ds} \qquad (5)$$

- **Wind input**

The basic assumption JANSSEN (1991) made, which was corroborated by his numerical results was that even for young wind sea, the wind profile has a logarithmic shape, though with a roughness length that depends on the wave-induced stress. As shown by MILES (1957), the growth rate of gravity waves due to wind then only depends on two parameters, namely

$$x = (u_*/c)\cos(\theta - \theta_w) \quad \text{and} \quad \Omega_m = \varkappa^2 g z_o / u_*^2$$

where $\varkappa$ is the von Karman constant, u_* is the friction velocity, c is the wave phase speed, θ_w is the wind direction and θ is the direction in which the waves propagate. The so-called profile parameter Ω_m characterizes the state of the mean air flow through its dependence on the roughness length z_o. Thus, through the profile parameter the growth rate depends on the roughness of the air flow, which, in its turn, depends on the sea state. A simple parameterization of the growth rate is of the form

$$\frac{\gamma}{\omega} = \varepsilon \beta x^2 \tag{6}$$

where γ is the growth rate, ω the angular frequency, ε the air-water density ratio and β the so-called Miles' parameter. The input source function of WAM model is given by

$$S_{in} = \gamma N \tag{7}$$

- **Dissipation source function**

The dissipation source function is based on the form:

$$S_{ds} = - C_{ds} \bar{\omega} \frac{k}{\bar{k}} \left[(1-\delta) + \delta \frac{k}{\bar{k}} \right] \left(\frac{\hat{\alpha}}{\hat{\alpha}_{PM}} \right)^P N \tag{8}$$

where $\bar{\omega}$ is the mean frequency, $k, \bar{k}$ are the wave and the mean wave number, $\hat{\alpha}$ is an integral wave steepness parameter defined by:

$$\hat{\alpha} = \bar{\omega}^4 g^{-2} \iint N(f,\theta) df \, d\theta \tag{9}$$

and $\hat{\alpha}_{PM}$ is the theoretical value of for a Pierson-Moskowitz spectrum. WAM4 assumes that $\delta = 0.5, p = 4$ and $C_{ds} = 4.5 \times 10^{-5}$ (KOMEN, *et al.,* 1994).

- **Nonlinear source function**

The nonlinear source function S_{nl} is represented by the discrete interaction operator parameterization proposed by HASSELMANN *et al.* (1985a,b). This retains the basic form of the exact nonlinear transfer function but it is reduced to a two-dimensional continuum by considering only a (mirror symmetrical) pair of discrete interaction configurations instead of taking into account all resonant quadruplets.

Extension to shallow water

In the standard WAM4 model code, the deep water transport equation (1) is extended to shallow water by including an additional source function S_{bf} representing the wave energy loss due to bottom friction and percolation. The other terms of the transport equation should also take into account the dependence on the depth D of the dispersion relation:

$$\omega = (gk \tanh k D)^{1/2} \tag{10}$$

Thus the following changes are assumed in the standard WAM4 code for the shallow water case:

- An additional bottom friction term is added to the left hand side of (5)
- The deep water group velocity in (2)-(4) is replaced by the group velocity for finite depth:
- Phase velocity is replaced by the appropriate value for finite depth
- Refraction term (4) is augmented to include the refraction due to variations of the water depth.
- The nonlinear source term for infinite depth is re-scaled.

Additionally to the standard model code, an extra source term has been added to the

right hand side of Eq.5 in order to parameterize the process of depth-induced wave breaking which can play a significant role in shallow water applications. The formulation of this term is based on the theory of BATTJES & JANSSEN (1978) who assumed that the probability distribution of breaking waves could be described as a Rayleigh distribution where the percentage Q_b of breaking waves is given as the solution of the relation

$$\frac{1-Q_b}{\ln Q_b} = -\left(\frac{H_{rms}}{H_{max}}\right)^2 \qquad (11)$$

where H_{rms} is the root mean square wave height and H_{max} the maximum wave height in the distribution assumed to be a fraction of the local water depth i.e. $H_{max}=0.8d$. The energy dissipation term S_{DWS} is then given by

$$S_{DWB} = -2Q_b\bar{f}\left(\frac{H_{max}}{H_{rms}}\right)^2 N \qquad (12)$$

where f is the average frequency of the wave spectrum.

Numerical scheme

The continuous wave spectrum is approximated in the numerical model by means of step functions which are constant in a frequency-direction bin. The size of the frequency-direction bin depends on frequency. A distinction is being made between a prognostic and a diagnostic part of the spectrum. The prognostic part has KL directional bands and ML frequency bands. These frequency bands follow a logarithmic scale, with $\Delta f / f = 0.1$, spanning a frequency range $f_{max}/f_{min} = (1.1)^{ML-1}$. The logarithmic scale has been chosen in order to have uniform relative resolution and also because the nonlinear transfer scales with frequency. The starting frequency may be selected in such a way that low-frequency swell is well resolved. For closed basins like the Mediterranean a choice of starting frequency of 0.05 Hz is sufficient.

Beyond the high-frequency limit of the prognostic part of the spectrum, a tail is added, with the same directional distribution as the last band of the prognostic region. Thus, the diagnostic part of the spectrum is given as:

$$N(f,\theta) = N(f_c,\theta)\left(\frac{f}{f_c}\right) \text{ for } f > f_c$$

The prognostic part of the spectrum is obtained by numerically solving the transport equation. The advective and refraction terms in the transport equation are solved using a first order upwinding scheme. Although such a scheme is characterized by a higher numerical diffusion (compared with a second order scheme, for example) it gives reasonable results and at the same time is simple and requires much less computer time and memory. For numerical stability the integration time step (propagation time step) must satisfy the inequality $\Delta t < \Delta x / c_g$ (CFL criterion). In order to reduce unrealistic energy loss at boundary points in cases where the waves propagate parallel to and near the coast, we followed the technique of MONBALIU *et al.* (2000) where an alternative octant propagation coordinate system was introduced in the original WAM4 code. For the octant advection scheme, eight propagation directions are defined instead of four in the quadrant scheme. More details can be found in MONBALIU *et al.* (2000) and in CAVALERI & SCLAVO (1998).

The WAVEWATCH-III model

WW3 (TOLMAN, 1997) is a third generation wave model developed at NOAA/NCEP, USA following the WAM

model development. However, WW3 differs from its predecessor in code structure (the WW3 code is written in FORTRAN 90, fully modular and allocatable), physical parameterizations and the numerical methods used for wave propagation. Moreover the model is fully parallelized (using the domain decomposition approach) and can be optionally compiled to include shared memory parallelisms using OpenMP compiler directives or Message Passing Interface directives for distributed memory environments. In this sense, it is an ideal candidate for high resolution applications where the computational load can be prohibitive for the WAM model. First or third order accurate numerical schemes are available to describe wave propagation (TOLMAN, 1995), which is considered to be linear, while relevant nonlinear effects such as resonant interactions are included in the source terms. The model includes two source term options, one based on the WAM – Cyle3 model philosophy (WAM3 Physics) and the other based on the formulation of TOLMAN & CHALIKOV (1996) (Tolman-Chalikov Physics). In both cases the source terms are integrated in time using a dynamically adjusted time stepping algorithm, which concentrates computational efforts on conditions with rapid spectral changes (TOLMAN, 1992; 1997; 1999). The governing equations of the model include refraction and straining of the wave field due to temporal and spatial variations of the mean water depth and the mean current (tides, surges etc.), and wave growth and decay due to the actions of wind, nonlinear resonant interactions, dissipation (whitecapping) and bottom friction. The model uses a regularly spaced grid in longitude and latitude. Wave spectrum is discretized using a constant directional increment (covering the entire circle), and a spatially varying wavenumber grid. The latter grid corresponds to an invariant logarithmic intrinsic frequency grid (TOLMAN & BOOIJ, 1998).

Setup of the wave hindcast/forecast system

Grid setup

The grid of the wave model for the Mediterranean Sea covers the geographical areas 7°W – 36°E and 30.25°N – 45.75°N as it is shown in Figure 1 with a resolution

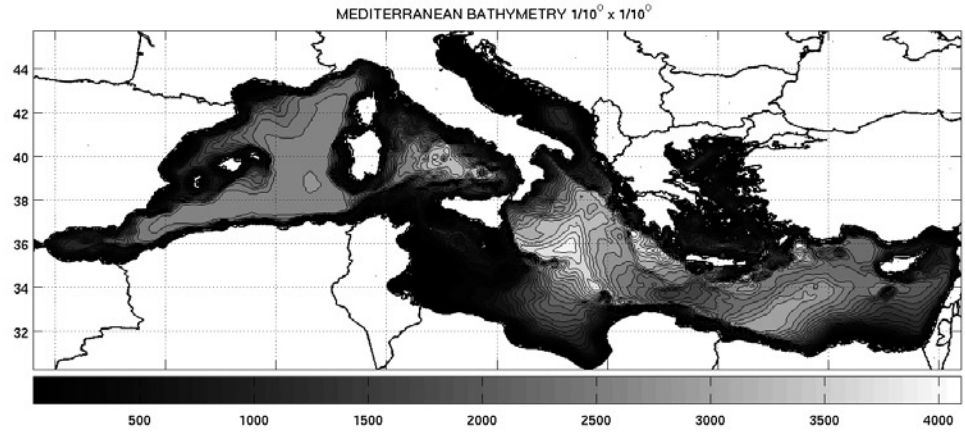

Fig. 1: Bathymetric map of the Mediterranean Sea as it is used by the WAM and WAVEWATCH models.

of 1/10° x 1/10°. The bathymetric map has been constructed from ETOPO 2 data (U.S. Department of Commerce, National Oceanic and Atmospheric Administration, National Geophysical Data Center, 2006; ***2-minute Gridded Global Relief Data***) using bi-linear interpolation and some degree of smoothing. In general the ETOPO2 data set, compared to the other well-known 2-minute resolution bathymetric data set DBDB2 (NRL, 2006), behaves better over the shelf bathymetric features, while DBDB2 has a much better representation of the coastlines. In any case, in shallow areas of the two basins local corrections were introduced, based on nautical charts issued by the Hellenic Naval Hydrographic Service.

The Mediterranean Sea WAM4 and WW3 models are implemented as standalone models since the Gibraltar open boundary is assumed to be closed. This is justified in the sense that no significant swell from the Atlantic Ocean is expected to propagate into the Mediterranean basin through Gibraltar Straits. The Dardanelles Straits are also considered as a closed boundary. The model uses 24 directional bins (15° directional resolution) and 30 frequency bins (ranging between 0.05Hz and 0.793Hz) to represent the wave spectra distribution. The model has been applied in shallow water mode but without depth and current refraction.

Wind input

A wave model input consists mainly of wind fields. The wave forecast system is one-way, coupled with the atmospheric forecast model ETA which runs operationally as part of the POSEIDON-II system. For the present study the atmospheric model was integrated from 01 January 2000 to 31 December 2001 with a horizontal grid increment of 0.10° in both directions, while the geographical extension of the model domain was set from 21.0° W to 51.0° E and from 24.4° N to 51.0° N as shown in Figure 2. In the vertical, 38 levels were used, stretching from ground to the model top. For the initial and the boundary meteorological conditions the ECMWF reanalysis gridded da-

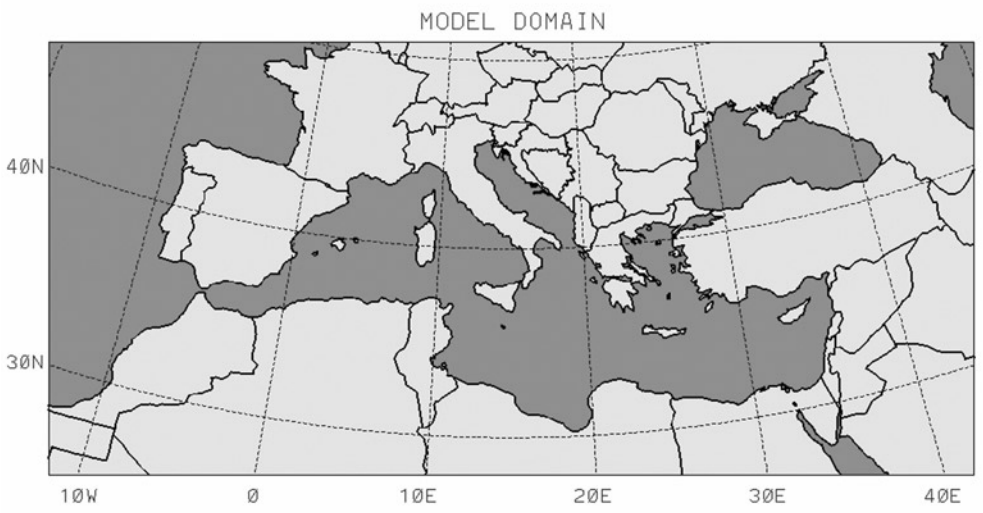

Fig. 2: The geographical coverage of the atmospheric model.

ta were used, in a 0.5˚ x 0.5˚ horizontal grid increment, for 16 standard pressure levels (1000, 925, 850, 700, 500, 400, 300, 250, 200, 150 and 100, 70, 50, 30, 20, and 10 hPa). The lateral boundaries of the model domain were updated at each time step from the ECMWF data available (linear interpolation). For the fields of the sea surface temperature and soil temperature and moisture, the ECMWF data, at a 0.5˚ x 0.5˚ horizontal grid increment were used.

A summary of the ETA model physics is given below:

- Viscous sublayer models over water and over land
- Surface layer scheme based on the similarity theory
- Mellor-Yamada level 2.5 turbulent exchange
- Betts-Miller-Janjic deep and shallow moist convection scheme
- Explicit cloud water/ice prediction
- OSU land surface scheme (4-layer soil scheme with vegetation)
- GFDL radiation

Model output can be summarized as follows:

- Air temperature at 2 m
- Relative humidity at 2 m
- Wind velocity at 10 m
- Precipitation
- Sea level pressure
- Net shortwave radiation at 0 m
- Downward longwave radiation at 0 m

Raw wind data (u,v components of the wind velocity) at 10 m above the sea surface are provided as input to the wave forecast system pre-processing programs along with the exact atmospheric model sea-land mask. Since the wave and wind grids, although of equal resolution, do not collocate, a spatial interpolation takes place in order to map the wind data onto the wave model grid. At each wave grid point the wind is evaluated by bi-linear interpolation from the four surrounding wind grid points previously masked with the atmospheric sea-land mask (elimination of land effects).

Analysis of the results

In this section we present a statistical analysis on wind and wave model hindcasts and buoy measurements respectively during a 2-year period (2000-2001). The significant wave height and the mean wave frequency/period used extensively in the section are defined as the n^{th} moments of the wave spectrum:

Significant wave height:

$$H_s = 4\sqrt{m_0} \tag{13}$$

Mean wave frequency:

$$f_{mean} = \sqrt{\frac{m_0}{m_2}} \tag{14}$$

with $m_n = \int_{f2}^{f2} f^n N(f) df$ where f_1 and f_2 are the lower and upper wave frequency limits. H_s is a measure of the combined sea and swell wave height and it is defined here as a spectral estimate (it can be shown that the spectral and the zero-crossing estimates of significant wave height are equivalent when the spectrum is narrow banded and the wave heights are described by the Rayleigh distribution). Finally another quantity used here is the peak wave period, which can be extracted directly from the wave spectrum.

Several measures can be used to describe the skill of a particular model forecast. In this paper we use the correlation skill score (CSS), the root mean square error (RMSE), the proportion of explained variance (PEV) and the bias (BIAS) defined as follows:

$$CSS = \frac{Cov(F,P)}{\sqrt{Var(F)Var(P)}} \quad (15)$$

$$RMSE = \sqrt{\{(F-P)^2\}} \quad (16)$$

$$PEV = \left(1 - \frac{Var(F-P)}{Var(P)}\right) \text{x } 100 \quad (17)$$

$$BIAS = <F-P> \quad (18)$$

In (15), (16) and (17) F stands for the model forecast and P for the verifying observation time series. For a perfect forecast, the correlation skill score is 1, the root mean squared error is zero and the proportion of explained variance (that is the percentage of P-variance explained by F) is 100%. If F is a random forecast with the same mean and variance as P, then the proportion of explained variance is -100% while the correlation skill score is zero.

The four buoy locations considered in this study here are shown in Figure 3:

Location 1: South-east of Santorini island (36° 15,4' – 25° 29,8' E, depth 308 m)
Location 2: West of Lesvos island (39° 09,13' – 25° 48,5' E, depth 125 m)
Location 3: North of Mykonos island (39° 30,58' – 25° 27,42' E, depth 141 m)
Location 4: South of the Athos peninsula (39° 57,81' – 24° 43,36' E, depth 220 m)

- Location 1: For the 2-year period (2000-2001) studied here, the mean significant wave height is 0.9 m, waves with significant height higher than 1.5 m occur with a probability of 14%, while the mean wave period is 3.7 sec. Maximum significant wave height recorded during 2000-2001 is 3.65 m.
- Location 2: For the 2-year period the mean significant wave height is 0.8m, waves with significant height higher than 1.5 m occur with a probability of 11%, while the mean wave period is 3.5 sec. Maximum significant wave height recorded during 2000-2001 is 4.92 m.

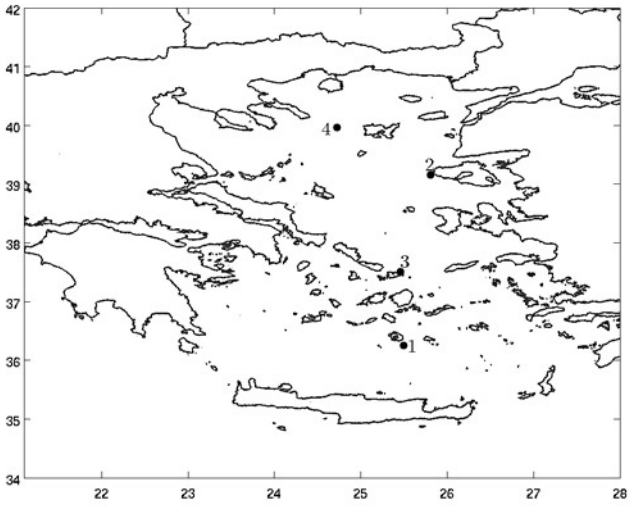

Fig. 3: Locations of the four buoy stations within the Aegean Sea (1: Santorini, 2: Lesvos, 3: Mykonos, 4: Athos).

- Location 3: For the 2-year period the mean significant wave height is 1.1m, waves with significant height higher than 1.5 m occur with a probability of 26%, while the mean wave period is 3.7 sec. Maximum significant wave height recorded during 2000-2001 is 4.83 m.
- Location 4: For the 2-year period the mean significant wave height is 0.8m, waves with significant height higher than 1.5 m occur with a probability of 16%, while the mean wave period is 3.6 sec. Maximum significant wave height recorded during 2000-2001 is 5.99 m.

The WW3 model offers two alternative options for setting the wind input source term and the wave dissipation term at the same time. The first option uses the parameterizations of TOLMAN & CHALIKOV (1996) while the second one follows the WAM Cycle-3 (WAM3) formulations for the two source terms. The former consists of the TOLMAN & CHALIKOV (1996) source term scheme, which comprises CHALIKOV & BELEVICH (1993) & CHALIKOV (1995) schemes for wave growth along with the dissipation scheme of TOLMAN & CHALIKOV (1996). Alternatively, the WAM3 formulation for the two terms involves equation

$$S_{in} = 0.25 \frac{\varrho_a}{\varrho_w} \max \left[0, \left(\frac{28 u_*}{0} \cos(\theta - \theta_w) \right) - 1 \right] \omega N \quad (20)$$

for the wind input term due to KOMEN *et al.* (1984) and equation (8) with $\delta = 0$, $p = 4$ and $C_{ds} = 2.36 \times 10^{-5}$ (KOMEN *et al.,* 1984) for the wave dissipation term.

In order to select the appropriate physics for the optimal representation of the Aegean Sea wave dynamics, we have performed two 1-year long (for year 2000) experiments using Tolman and Chalikov in the first and WAM3 formulations in the second experiment. Results from these runs for the four buoy locations are presented in Table 1 in terms of the correlation skill score (CSS), the root mean squared error (RMSE) and the proportion of explained variance (PEV) regarding the significant wave height as simulated by the WW3 model, following the two formulations. In terms of the correlation skill score, the two formulations show almost the same behavior for all buoy locations. However the significant wave height RMS error related to WAM3 formulation is improved with respect to TOLMAN &

Table 1
WW3 model: Tolman versus WAM3 physics for year 2000 simulation.

Sign. Wave height-WW3	CSS	RMSE (meters)	PEV
Location 1 Tolman / WAM3 Physics	0.862 / 0.857	0.49 / 0.37	68.2% / 72.9%
Location 2 Tolman / WAM3 Physics	0.855 / 0.883	0.47 / 0.34	67.2% / 77.2%
Location 3 Tolman / WAM3 Physics	0.846 / 0.831	0.68 / 0.55	63.6% / 67.5%
Location 4 Tolman / WAM3 Physics	0.823 / 0.851	0.57 / 0.46	58.5% / 67.9%

CHALIKOV physics option. A more significant improvement is evident in the proportion of explained variance which for buoy locations 2 & 4 is higher by 10% for WAM3 formulation. As our main scope here is to optimize the model behavior for the Aegean Sea region, we conclude that the WAM3 physics formulation is the most appropriate one for the WW3 model implementation and will be used henceforth.

Figures 4a, 5a, 6a and 7a present scatter plots of measured significant wave heights versus WAM4 model simulations for the four buoy locations over the two year (2000-2001) period. WW3 respective scatter plots are shown in Figures 8a, 9a, 10a and 11a. The diagonal lines denote a perfect fit of model and observed values. Mean wave period scatter plots are shown in Figures 4b, 5b, 6b and 7b for the WAM4 model and Figures 8b, 9b, 10b and 11b for the WW3 model, respectively. In order to have a picture of the atmospheric model skill we present the respective scatter plots for the wind speed in Figures 4c, 5c, 6c and 7c. In each of the diagrams presented in Figures 4-11 we additionally show the slope ***b*** and the intercept ***a*** corresponding to the linear regression of observed data over the model predictions. Statistics CSS, RMSE, PEV and BIAS are shown in Tables 3a (significant wave height) and 3b (mean wave period) for the WAM4 model and Tables 4a and 4b for the WW3 model respectively. These statistics were calculated over the two year period 2000-2001. The four statistics (CSS, RMSE, PEV and BIAS) for the wind speed are shown in Table 2.

The common characteristics of the significant wave height scatter plot diagrams for the WAM4 and WW3 models and for buoy locations 1-3 is that both models tend

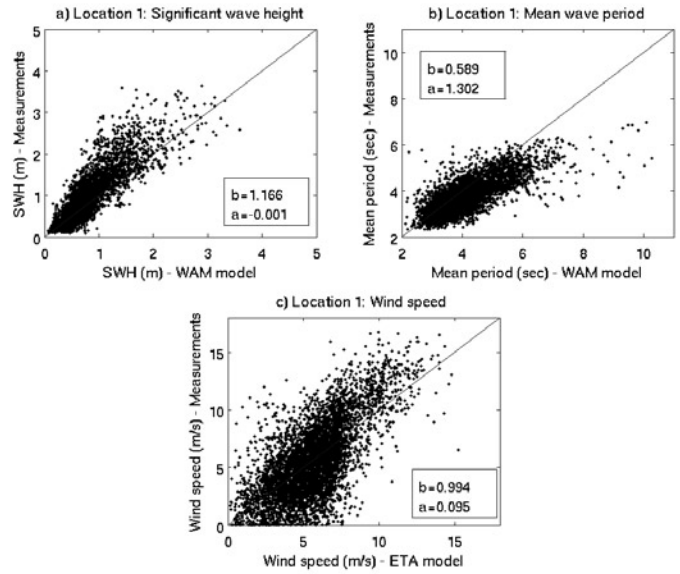

Fig. 4: Scatter plot of a) significant wave height, b) mean wave period and c) wind speed from measurements and WAM4 (a-b) or ETA (c) model hindcasts (2000-2001) for location 1 (Santorini buoy). In each box, the slope *b* and the intercept *a* corresponding to the linear regression of observed data over the model predictions are presented.

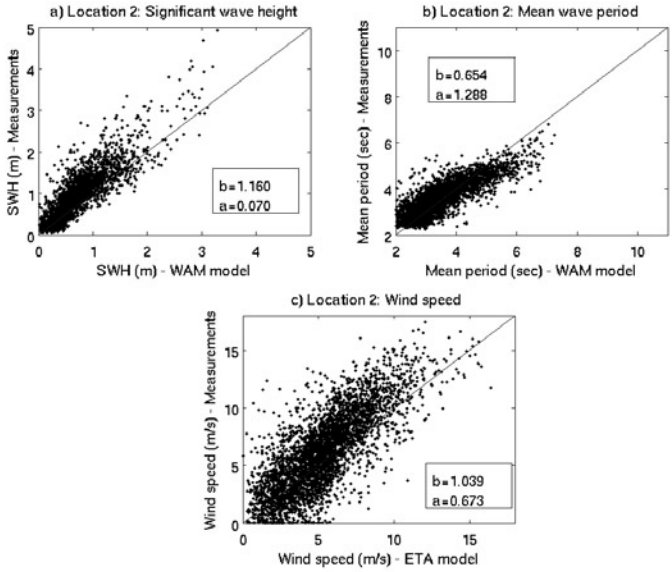

Fig. 5: Scatter plot of a) significant wave height, b) mean wave period and c) wind speed from measurements and WAM4 (a-b) or ETA (c) model hindcasts (2000-2001) for location 2 (Lesvos buoy). In each box, the slope *b* and the intercept *a* corresponding to the linear regression of observed data over the model predictions are presented.

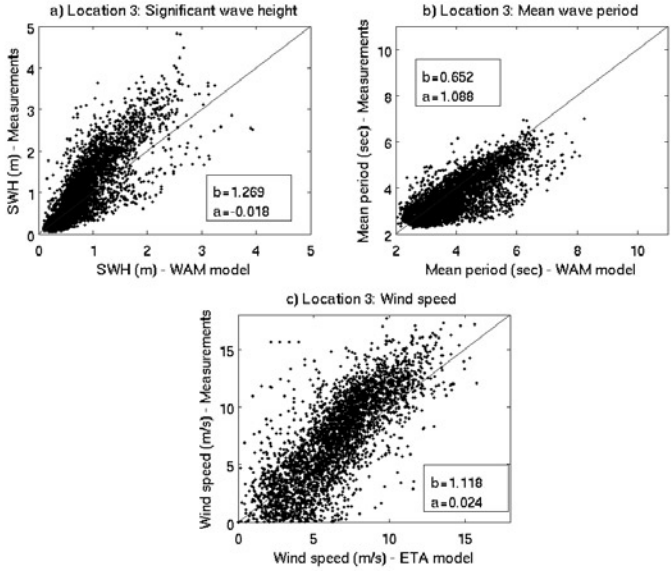

Fig. 6: Scatter plot of a) significant wave height, b) mean wave period and c) wind speed from measurements and WAM4 (a-b) or ETA (c) model hindcasts (2000-2001) for location 3 (Mykonos buoy). In each box, the slope *b* and the intercept *a* corresponding to the linear regression of observed data over the model predictions are presented.

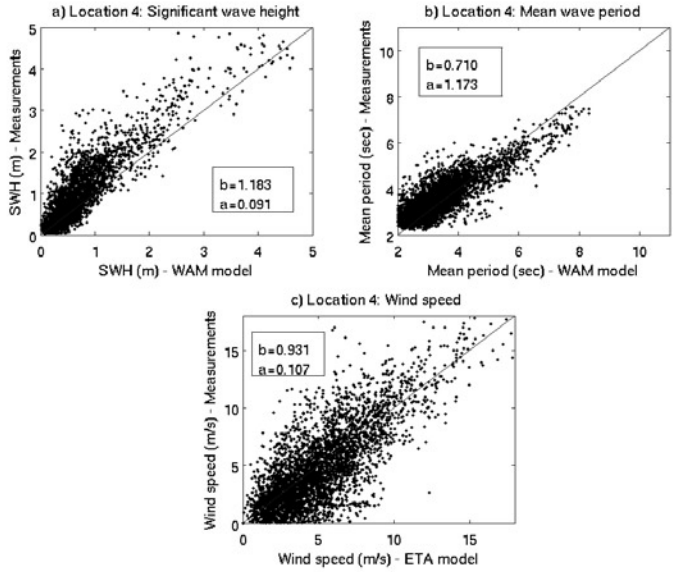

Fig. 7: Scatter plot of a) significant wave height, b) mean wave period and c) wind speed from measurements and WAM4 (a-b) or ETA (c) model hindcasts (2000-2001) for location 4 (Athos buoy). In each box, the slope *b* and the intercept *a* corresponding to the linear regression of observed data over the model predictions are presented.

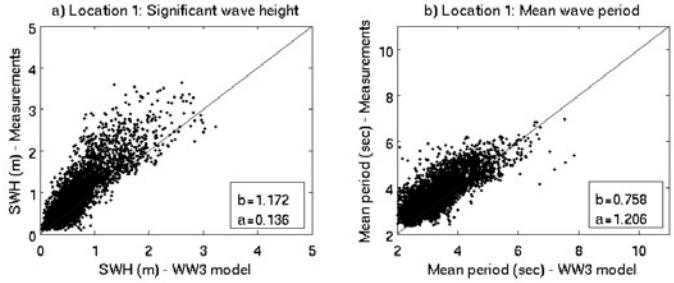

Fig. 8: Scatter plot of a) significant wave height and b) mean wave period from measurements and WW3 model hindcasts (2000-2001) for location 1 (Santorini buoy). In each box, the slope *b* and the intercept *a* corresponding to the linear regression of observed data over the model predictions are presented.

to underestimate wave energy for waves with significant wave heights higher than 2 m, while below this threshold both models produce balanced forecasts in accordance with the measurements. This can be also seen from the conditional skill scores presented in Tables 5a-5b (WAM4 model) and 5c-5d (WW3 model) for the first three buoy locations, while for location 4 (Athos buoy) the models show almost equal skill in both low (<2 m) and high (>2 m) significant wave height regimes. This behav-

Table 2
Statistics for the simulated wind speed at the four buoy locations.

Wind speed	CSS	RMSE (m/s)	PEV	BIAS (m/s)
Location 1	0.684	2.37	46.8%	-0.06
Location 2	0.777	2.33	60.3%	-0.88
Location 3	0.792	2.56	61.3%	-0.74
Location 4	0.780	2.23	60.4%	0.23

Table 3a
Statistics for the WAM4 simulated significant wave height at the four buoy locations.

Sign. Wave height-WAM4	CSS	RMSE (meters)	PEV	BIAS (meters)
Location 1	0.855	0.33	71.7%	-0.12
Location 2	0.878	0.33	75.8%	-0.17
Location 3	0.821	0.52	64.4%	-0.20
Location 4	0.902	0.42	79.4%	-0.20

Table 3b
Statistics for the WAM4 simulated mean wave period at the four buoy locations.

Mean wave period-WAM4	CSS	RMSE (sec)	PEV	BIAS (sec)
Location 1	0.777	0.70	30.8%	0.37
Location 2	0.828	0.52	49.5%	-0.09
Location 3	0.752	0.73	40.5%	0.29
Location 4	0.837	0.59	58.4%	-0.19

iour can be partially explained by considering the reliability of the model predicted winds as shown in Tables 6a and 6b. Of course in this approach we have to bear in mind that the higher waves could have been generated by a strong wind in an area far from the stations, or even in a time period before the measured waves. In Table 6a we have calculated the CSS, RMSE, PEV and BIAS statistics for winds corresponding to wave height conditions lower than 2 m. In all four buoy locations, the model simulated winds used to drive the wave models have a CSS between 0.61-0.75 and a bias not higher than 0.85 m/s. As a result, the wave models show a very good skill in this range (0-2 m) of simulated wave heights. On the other hand, the skill of the predicted winds decreases for the first three buoy locations when the statistics are calculated for wave heights higher than 2 m (Table 6b). In response, the skill of the wave models decreases for this range of wave heights. The exceptional behaviour of buoy location 4 can be explained as well. Comparing Tables 6a and 6b for this buoy location, it is clear that the wind statistics for wave heights higher than 2 m are the same or even better than those that correspond to the range of wave heights 0-2 m.

Table 4a
Statistics for the WW3 simulated significant wave height at the four buoy locations.

Sign. Wave height-WW3	CSS	RMSE (meters)	PEV	BIAS (meters)
Location 1	0.85	0.39	70.8%	-0.25
Location 2	0.885	0.36	77.3%	-0.24
Location 3	0.834	0.55	67.8%	-0.30
Location 4	0.910	0.45	80.8%	-0.28

Table 4b
Statistics for the WW3 simulated mean wave period at the four buoy locations.

Mean wave period – WW3	CSS	RMSE (sec)	PEV	BIAS (sec)
Location 1	0.768	0.64	53.15%	-0.40
Location 2	0.831	0.76	57.1%	-0.59
Location 3	0.792	0.70	55.21%	-0.39
Location 4	0.850	0.87	65.6%	-0.70

Table 5a
Wave height classification (<2 m).

Sign Wave height – WAM4	CSS	RMSE (meters)	PEV	BIAS (meters)
Location 1	0.813	0.26	66.0%	-0.08
Location 2	0.845	0.29	71.1%	-0.15
Location 3	0.711	0.38	50.6%	-0.09
Location 4	0.799	0.34	62.0%	-0.16

Table 5b
Wave height classification (>2 m).

Sign Wave height – WAM4	CSS	RMSE (meters)	PEV	BIAS (meters)
Location 1	0.418	0.86	-97.6%	-0.69
Location 2	0.685	0.91	29.9%	-0.77
Location 3	0.569	1.02	2.8%	-0.91
Location 4	0.850	0.94	63.1%	-0.76

An interesting characteristic of the scatter plot diagrams presented in figures 4b – 11b and Tables 3b and 4b is that the WAM4 model tends to overestimate the mean wave period (max bias of 0.37 sec for buoy location 1) while the WW3 model tends to underestimate wave periods (max bias of -0.70 sec for buoy location 4). In general the WW3 model shows a larger bias compared to the WAM4 model although PEV statistic is

Table 5c
Wave height classification (<2 m).

Sign Wave height – WW3	CSS	RMSE (meters)	PEV	BIAS (meters)
Location 1	0.807	0.32	64.9%	-0.20
Location 2	0.845	0.29	71.1%	-0.15
Location 3	0.726	0.41	52.6%	-0.19
Location 4	0.807	0.38	64.2%	-0.23

Table 5d
Wave height classification (>2 m).

Sign Wave height – WW3	CSS	RMSE (meters)	PEV	BIAS (meters)
Location 1	0.410	0.97	-91.4%	-0.83
Location 2	0.669	0.97	32.2%	-0.84
Location 3	0.595	1.05	7.7%	-0.95
Location 4	0.842	0.98	67.2%	-0.83

Table 6a
Winds corresponding to wave heights <2 m.

Wind speed	CSS	RMSE (m/s)	PEV	BIAS (m/s)
Location 1	0.614	2.31	37.2%	0.07
Location 2	0.751	2.31	56.4%	-0.85
Location 3	0.733	2.41	53.5%	-0.44
Location 4	0.660	2.21	41.5%	0.29

Table 6b
Winds corresponding to wave heights >2 m.

Wind speed	CSS	RMSE (m/s)	PEV	BIAS (m/s)
Location 1	0.450	3.18	1.0%	-2.11
Location 2	0.462	3.15	2.2%	-1.73
Location 3	0.367	3.27	-29.5%	-2.42
Location 4	0.728	2.53	44.6%	-0.64

higher for the WW3 model.

From the scatter diagram of Figure 4c (buoy location 1) we note that the simulated winds tend to be accurate at the speed range of 4-8 m/s (such winds occur with a probability of 44%, while their estimated bias is -0.11 m/s), to underestimate reality for speeds higher than 8 m/s (23% occurrence – estimated bias is -0.56 m/s) and to do the opposite for values lower than 4 m/s (33% occurrence – estimated bias is 0.62 m/s). As a result, the overall correlation skill score is 0.68 while the percentage of explained variance is 46.8%. For the same lo-

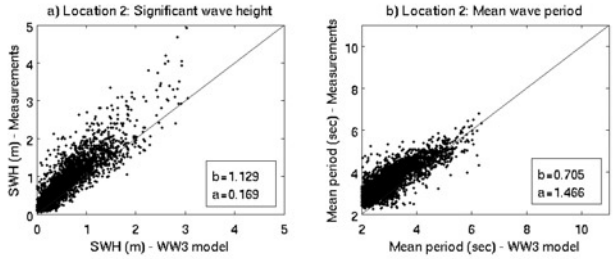

Fig. 9: Scatter plot of a) significant wave height and b) mean wave period from measurements and WW3 model hindcasts (2000-2001) for location 2 (Lesvos buoy). In each box, the slope *b* and the intercept *a* corresponding to the linear regression of observed data over the model predictions are presented.

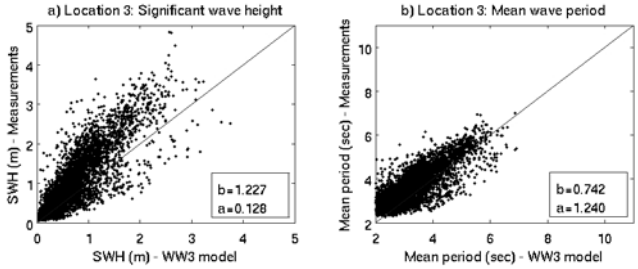

Fig. 10: Scatter plot of a) significant wave height and b) mean wave period from measurements and WW3 model hindcasts (2000-2001) for location 3 (Mykonos buoy). In each box, the slope *b* and the intercept *a* corresponding to the linear regression of observed data over the model predictions are presented.

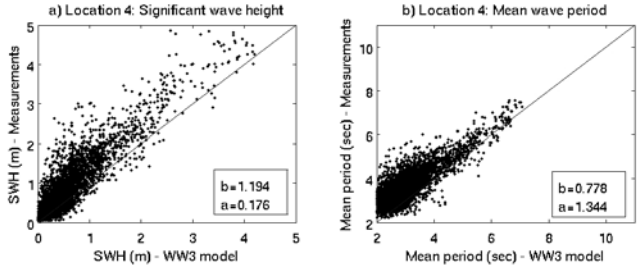

Fig. 11: Scatter plot of a) significant wave height and b) mean wave period from measurements and WW3 model hindcasts (2000-2001) for location 4 (Athos buoy). In each box, the slope *b* and the intercept *a* corresponding to the linear regression of observed data over the model predictions are presented.

cation, both wave models show the same behaviour in terms of the simulated significant wave height resulting in a correlation skill score of 0.85 and an RMS error of 0.3-0.4m. Both models underestimate wave heights (bias of -0.12 and -0.25 for WAM4 and WW3

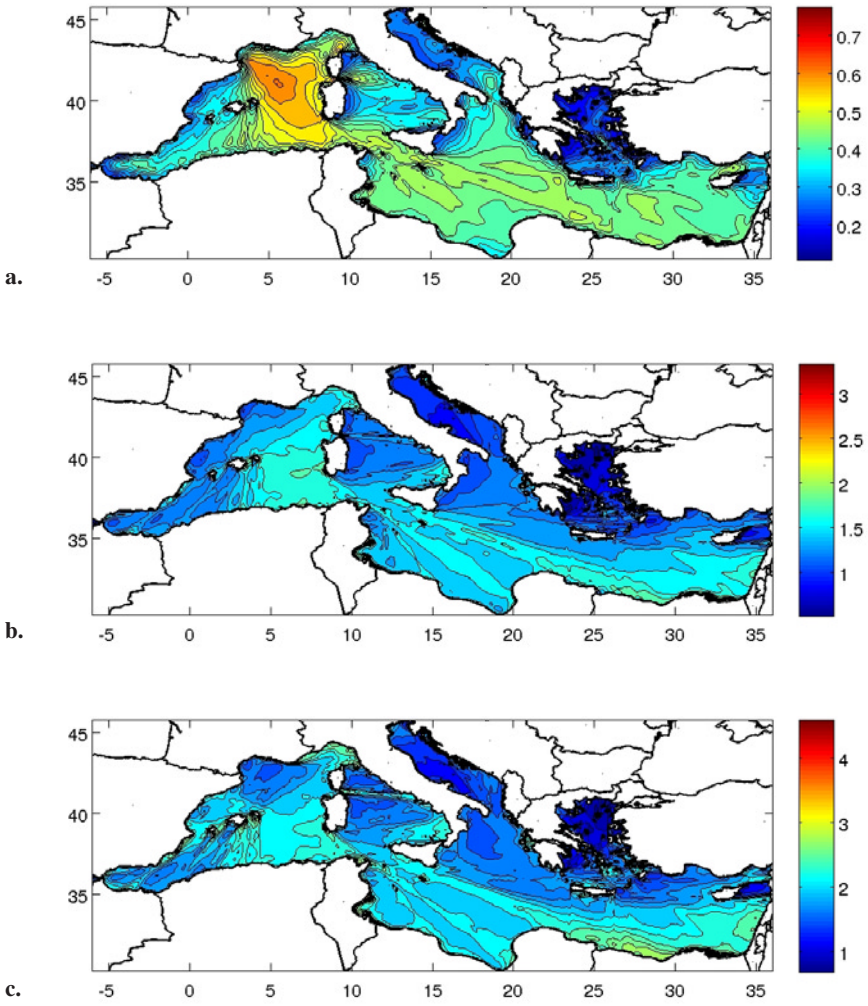

Fig. 12: a) RMS difference (in meters) of WAM4 and WW3 significant wave height over 2000-2001 b) RMS difference (in sec) of WAM4 and WW3 mean wave period over 2000-2001 c) RMS difference (in sec) of WAM4 and WW3 peak wave period over 2000-2001.

respectively) which is more pronounced for waves higher than 2 m. Thus, although the correlation skill score is ~0.81 for both models for significant wave heights lower than 2 m, it reduces to 0.41 when one considers significant wave heights higher than 2 m. We argue that this behaviour is related to the wind speed bias (underestimation) that characterizes wind speeds higher than 8 m/s. As shown in Table 6b, the winds corresponding to significant wave heights larger than 2m are characterized by poor statistics: the CSS is 0.45 while PEV approaches to zero. The two wave models perform differently in terms of the mean wave period, although they are both characterized by a CSS of 0.77. More

specifically, the WAM4 model shows a slight overestimation of the wave period over the whole range of values (bias of 0.37 sec) while WW3 shows the opposite behaviour, underestimating mean wave periods (overall bias is -0.4 sec). However the WW3 model explains 53% of the mean wave period variance while this figure is lowered to 31% for the WAM4 model.

The wind speed scatter diagram of Figure 5c (buoy location 2) presents two areas of distinct wind speed characteristics: for observed wind speeds lower than 7 m/s which occur with a frequency of 60%, the atmospheric model simulation is very accurate with an overall bias of 0.03 m/s, while for wind speeds higher than 7 m/s the simulated winds underestimate reality (estimated bias is -0.9 m/s). The overall CSS for this location is 0.77 while the percentage of explained variance exceeds 60% (Table 2). In terms of the simulated significant wave height, the two wave models bear almost the same characteristics, with a CSS of 0.88, RMS error ranging between 0.33-0.36 meters and explained variance of 76-77%. Both models underestimate the significant wave height (overall bias is -0.17 m and -0.24 m for the WAM4 and WW3 models respectively) which for the WAM4 model is evident for wave heights higher than 1m while for the WW3 model this underestimation starts even from lower values. The CSS is 0.56-0.59 for significant wave heights larger than 2 m, PEV is lower than 10% while the bias is larger than -0.9m for both wave models. Again the wave energy underestimation for this range of wave heights can possibly be attributed to the atmospheric model performance in terms of the wind speed forecast, as can be seen from Table 6b.

For buoy location 3, the wind scatter diagram shown in Figure 6c presents two areas of distinct behaviour: a) for observed winds in the range 0-6m/s occurring at 33% the model simulation is accurate (estimated bias is -0.37m/s) and b) wind speeds higher than 6m/s which dominate the climate of Mykonos (67% occurrence) are underestimated by the model as the estimated bias is -2.6 m/s. In terms of the simulated significant wave height, the two wave models bear almost the same characteristics with a CSS of ~0.83, RMS error ranging between 0.52-0.55 meters and explained variance of 64-68%. Overall, the two wave models underestimate the observed significant wave height time series by 0.2-0.3 m. The underestimation is more pronounced for wave heights higher than 2 m and such behaviour can be attributed partially to the underestimation of the wind speeds at this location. In fact, as can be seen from Table 6b, the CSS statistic is very low (0.36) while the proportion of explained variance becomes negative. In terms of the wave period, we see again an opposite behaviour from the two models: the WAM4 model overestimates wave periods by 0.29 sec while the WW3 model underestimates it by 0.39 sec on average. The rest of the statistics (CSS, RMSE and PEV) related to the mean wave period statistics are comparable for the two models.

Buoy location 4 has the second highest PEV in terms of the simulated wind speed out of the four locations (60.4%). The simulated winds for this location are characterized by an RMS error of 2.23 m/s and a correlation skill score of 0.78. The simulated wave heights and wave periods from the two models are characterized by high correlation skill scores ~0.9 for significant wave height and ~0.85 for the mean wave period. For this buoy location the two models show high and comparable skill score in predicting waves either lower or higher than 2m (Tables 5a and 5b). The significant wave

height bias is negative and comparable for WAM4 and WW3 (-0.2m and -0.28m respectively) while both models underestimate the mean wave period although this behaviour is more pronounced for the WW3 model (-0.19 sec and -0.7 sec). As noted before, the success of the two wave models in the two wave height regimes can very well be attributed to the wind reliability, as can be deduced by inspecting Tables 6a and 6b. In particular, for this buoy location the wind CSS is 0.66 for significant wave heights lower than 2m and becomes even higher for significant wave heights greater than this value. It is also of interest that the proportion of explained variance is sustained at values higher than 40% for both wave regimes, while the bias is the lowest out of the four locations.

The differences between the WAM4 and WW3 models can be additionally assessed over the whole modelling domain by inspecting the RMS differences of significant wave height, mean period and peak wave period presented in Figures 12a - 12c. In terms of significant wave height, the two models perform almost identically in the Tyrrhenian, Adriatic and Aegean Seas and the Alboran and Balearic basins. These areas are mostly dominated by wind seas and it is reasonable to assume that both models present equivalent skill in this part of the wave spectra. This is also evident from Figure 12b and 12c where again the differences in wave periods and in the same geographic areas are minimal between the two models. Differences exist in the Algerian basin, the central and, more pronouncedly, in the north part of the Provencal basin (max RMS difference of 0.7m), the central Ionian and the central Levantine basin. These geographic areas coincide with the passage of the major cyclonic systems over the Mediterranean basin and it is most likely that they are affected by swell systems propagation. Additionally, the central and the northern part of the Provencal basin is the area dominated by the Mistral wind circulation.

Summary and Discussion

In this study, two state of the art, third generation wave models, a modified version of the WAM4 and the WW3 models were applied in hindcast mode to simulate the wave regime in the Mediterranean Sea for a 2-year (2000-2001) evaluation period. This is an interesting exercise as a systematic inter-comparison of wave model results is not often reported, especially for the Mediterranean region. The models were adapted exactly on the same spatial, directional and frequency grids and were additionally set to shallow water mode without, however, depth and current refraction. The wind fields used to drive the models were provided on a 3-hour basis from an ETA atmospheric model implementation with a 0.1˚x 0.1˚ resolution which downscaled the ECMWF 0.5˚x 0.5˚ re-analysis for the same time period. Before any intercomparison between the two models, the first step was to tune the WW3 model in order to optimize its performance within the Aegean Sea, this being the area of prime interest. For that purpose, the WW3 model was integrated twice for the year 2000, using the WAM3 and Tolman-Chalikov physics options, respectively. Inter-comparison of the WW3 model results from this exercise, with available observations at the four buoy locations of the POSEIDON observational network, showed that in terms of significant wave height and peak wave period, the WW3 model using WAM3 physics source terms performs slightly better than when the Tolman-Chalikov source term is activated. Next the results of the WAM4

and WW3 (using the WAM3 physics source term as default) model simulations for the period 2000-2001 were validated against the available significant wave height and mean wave period buoy observations at four characteristic locations within the Aegean Sea. Both models provided skilful hindcasts characterized by similar statistics. It was found that the WW3 model systematically underestimates the wave period, while the opposite tendency was found for the WAM4 model, but not for all buoy locations. The significant wave height skill scores range between 0.82 and 0.91 for the two models over the four buoy locations (RMSE 0.33-0.55m), while the skill scores for the mean wave period are in the range of 0.77-0.85 (RMSE 0.52-0.87sec). At the same time the wind speed skill scores are lower, ranging between 0.6 and 0.8. For the first three buoy locations, the wind statistics become very poor (skill scores between 0.36-0.45 and close to zero or negative proportion of explained variance) when one considers wave regimes with significant wave heights higher than 2 m. This poor performance of the atmospheric model affects in turn the quality of the wave forecasts. For the open sea buoy of Athos (buoy location 4) the situation is rather different, as both wind and wave forecasts show a very pronounced skill either below or higher than 2 m significant wave heights.

The study of the scatter plot diagrams showed that both wave models tend to underestimate the significant wave height although this behaviour is more pronounced for the WW3 model. As noted before, a noticeable feature coming out from the wave and atmospheric forecasts is the low proportion of observed variance explained by the models (wave and atmospheric) as far as the mean wave period and the wind speed are concerned. Finally, the inter-comparison of the two wave models over the whole Mediterranean basin showed that noticeable differences in terms of significant wave height and periods (significant wave height RMS differences of 0.5-0.7m and wave period RMS differences of 1.5-2 sec) exist along the track of the main cyclones over the basin, where the swell contribution to the wave field is important. On the other hand, in the geographic areas of the Mediterranean Sea where wind seas dominate, the two models exhibit almost the same performance. This result shows also the areas where the wave data assimilation is expected to have a positive impact as it is generally accepted that the wave assimilation process can efficiently affect the swell dominated part of the wave spectra.

Future developments will concentrate on the data assimilation problem of in situ and remotely sensed wave height measurements. In a parallel effort, research will be devoted to implementing a two-way coupling between the wave and the atmospheric models in terms of the surface roughness length. In areas like the Mediterranean Sea where the wind sea dictates the shape of the wave spectrum, such a coupling approach is expected to affect the quality of both the wind and wave forecasts.

Acknowledgements

This study was carried out with financial support from POSEIDON-II and ESPEN (An Enhanced Operational System for Wave Monitoring and Prediction with Applications in Hellenic Navigation) research projects.

References

ARDHUIN, F., RASCLE, N. & BELI-
BASSAKIS, K.A., 2008. Explicit wave-

averaged primitive equations using a generalized Lagrangian mean. *Ocean Modelling,* 20 (1): 35-60.

BATTJES, J.A. & JANSSEN, J.P.F.M., 1978. Energy loss and set-up due to breaking of random waves. p.569-587. In: *Proceedings of the International Conference on Coastal Engineering,* ASCE, New York.

CAVALERI, L. & SCLAVO, M., 1998. Characteristics of the quadrant and octant advections schmes in wave models. *Coastal Engineering,* 34 (3-4): 221-242.

CHALIKOV, D.V., 1995. The parameterization of the wave boundary layer. *Journal of Physical Oceanography,* 25: 1333-1349.

CHALIKOV, D.V. & BELEVICH, M.Yu., 1993. One dimensional theory of the wave boundary layer. *Boundary Layer Meteorology,* 63 (1-2): 65-96.

HASSELMANN, S., HASSELMANN, K., BAUER, E., BERTOTTI, L., CARDONE, C.V., EWING, J.A., GREENWOOD, J.A., GUILLAUME, A., JANSSEN, P.A.E.M., KOMEN, G.J., LIONELLO, P., REISTAD, M. & ZAMBRESKY, L., 1988. The WAM Model - a third generation ocean wave prediction model. *Journal of Physical Oceanography,* 18 (12): 1775-1810.

HASSELMANN, S. & HASSELMANN, K., 1985a. Computations and parameterizations of the nonlinear energy transfer in a gravity wave spectrum. Part I: A new method for efficient computations of the exact nonlinear transfer integral. *Journal of Physical Oceanography,* 15 (11): 1369-1377.

HASSELMANN, S., HASSELMANN, K., ALLENDER, J.H. & BARNETT, T.P., 1985b. Computations and parameterizations of the nonlinear energy transfer in a gravity wave spectrum. Part II: Parameterizations of the nonlinear energy transfer for application in wave models. *Journal of Physical Oceanography,* 15 (11): 1378-1391.

HERSBACH, H. & JANSSEN, P.A.E.M., 1999. Improvement of the Short-Fetch behavior in the Wave Ocean Model (WAM). *Journal of Atmospheric and Oceanic Technology,* 16: 884-892.

KOMEN, G.J., HASSELMANN, S. & HASSELMANN, K., 1984. On the existence of a fully developed wind-sea spectrum. *Journal of Physical Oceanography,* 14: 1271-1285.

KOMEN, G.J., CAVALERI, L., DONELAN, M., HASSELMANN, K., HASSELMANN, S. & JANSSEN, P.A.E.M., 1994. *Dynamics and modeling of ocean waves.* Cambridge University Press, 532 pp.

JANSSEN, P.A.E.M., 1991. Quasi-Linear theory of wind wave generation applied to wave forecasting. *Journal of Physical Oceanography,* 21 (11): 1631-1642.

MELLOR, G., 2003. The three-dimensional current and surface wave equations. *Journal of Physical Oceanography,* 33: 1978-1989.

MILES, J.W., 1957. On the generation of surface waves by shear flow. Journal of Fluid Mechanics, 3 (2): 185-204.

MONBALIU, J., HARGREAVES, R., ALBIACH, J., LUO, W., SCLAVO M. & GÜNTHER, H., 2000. The spectral wave model, WAM, adapted for applications with high spatial resolution. *Coastal Engineering,* 41 (1-3): 41-62.

NITTIS, K., PERIVOLIOTIS, L., BALLAS, D., KORRES, G., SOUKISSIAN, T., PAPADOPOULOS, A., GEORGOPOULOS, D., MALLIOS, A.,

TRIANTAFYLLOU, G., POLLANI, A., ZERVAKIS, V., PAPATHANASSIOU V. & CHRONIS, G., 2005. POSEIDON-II: A second generation monitoring and forecasting system for the Eastern Mediterranean. p.585-590. In: *4th EuroGOOS Conference on European Operational Oceanography: Present and Future,* 6-9 June, Brest, France.

NRL, 2006. Digital bathymetry data base 2-minute resolution v.3 (DBDB2). http://www7320.nrlssc.navy.mil/DBDB2 WWW/NRLCOM dbdb2.html.

PERRIE, W., TANG, C., HU, Y. & DETRACY, B.M., 2003. The impact of waves on surface currents. *Journal of Physical Oceanography,* 33: 2126-2140.

PIERSON, W.J., & MOSKOWITZ, L., 1964. A proposed spectral form for fully developed wind seas based on the similarity theory of S.A.Kitaigorodskii. *Journal of Geophysical Research,* 69 (24): 5181-5203.

SOUKISSIAN, T., HATZINAKI, M., KORRES, G., PAPADOPOULOS, A., KALLOS, G. & ANADRANISTAKIS, E., 2007. *Wind and Wave Atlas of the Hellenic Seas.* Athens, Hellenic Centre for Marine Research Publications, 300 pp.

TOLMAN, H.L. & BOOIJ, N., 1998. Modeling wind waves using wavenumber-direction spectra and a variable wavenumber grid. *Global Atmosphere & Ocean System,* 6 (4): 295-309.

TOLMAN, H.L., 1997. *User manual and system documentation of WAVEWATCH-III version 1.15.* NOAA / NWS / NCEP OMB Technical Note 151, 97 pp.

TOLMAN, H.L., 1995. Sub-grid modeling of moveable-bed bottom-friction in wind-wave models. *Coastal Engineering,* 26: 57-75.

TOLMAN, H.L. & CHALIKOV, D., 1996. Source terms in a third-generation wind-wave model. *Journal of Physical Oceanography,* 26: 2497-2518.

TOLMAN, H.L., 1992. Effects of numerics on the physics in a third generation wind-wave model. *Journal of Physical Oceanography,* 22: 1095-1111.

WU, J., 1982. Wind-stress coefficients over sea surface from breeze to hurricane. *Journal of Geophysical Research,* 87 (C12): 9704-9706.